Snapshot retinal imaging Mueller matrix polarimeter

Yifan Wang*[a], Michael Kudenov[a], Amir H. Kashani[b], Jim Schwiegerling[c], Michael Escuti[a]
[a]Department of Electrical and Computer Engineering, North Carolina State University, 2410 Campus Shore Dr, Raleigh, NC USA 27606; [b]USC Eye Institute, Keck School of Medicine of USC, 1975 Zonal Ave. Los Angeles, CA USA 90033; [c]College of Optical Sciences, University of Arizona, 1630 East University Blvd, Tucson, AZ, USA 85721

ABSTRACT

Early diagnosis of glaucoma, which is a leading cause for visual impairment, is critical for successful treatment. It has been shown that Imaging polarimetry has advantages in early detection of structural changes in the retina. Here, we theoretically and experimentally present a snapshot Mueller Matrix Polarimeter fundus camera, which has the potential to record the polarization-altering characteristics of retina with a single snapshot. It is made by incorporating polarization gratings into a fundus camera design. Complete Mueller Matrix data sets can be obtained by analyzing the polarization fringes projected onto the image plane. In this paper, we describe the experimental implementation of the snapshot retinal imaging Mueller matrix polarimeter (SRIMMP), highlight issues related to calibration, and provide preliminary images acquired from the camera.

Keywords: Glaucoma, polarimeter, snapshot, Mueller matrix, fundus camera

1. INTRODUCTION

The incidence of glaucoma has been growing rapidly and it is one of the leading causes of blindness in the world. By 2020, roughly 80 million of global population will be diagnosed with glaucoma, and about 14% percent of these patients will suffer from bilateral blindness[1]. Since glaucoma can be treated to prevent or slow progression, early diagnosis is essential for vision preservation. The common methods of glaucoma diagnosis are based on the detection of structural and functional changes with fundus photography and perimetry. However, these kinds of tests are not sensitive for detection of early disease and, in some cases, are not easily reproducible or reliable[2]. Many studies have demonstrated that abnormalities in the retinal nerve fiber layer (RNFL) are the earliest signs of glaucoma[3]. Over the years, this has inspired the developments of various retinal imaging modalities, including confocal scanning laser ophthalmoscopy (cSLO), optical coherence tomography (OCT), and scanning laser polarimetry (SLP) [4]. While most of these imaging modalities focus on the peripapillary RNFL thickness loss, SLP is unique because it is based on cytoskeletal birefringence[5], which is thought to be more sensitive than RNFL thickness for detection of early disease. This suggests that birefringence may be a functional measure of declining axonal health before tissue loss, and therefore more sensitive at detecting RNFL disease. However, SLP also has its limitations: first, the temporal resolution of SLP is relatively low because of its detecting mechanism; and second, many commercially available SLPs are partial polarimeters, which means they only measure a subset of the whole polarization information of retina. This makes corneal birefringence compensation more challenging to implement, especially on distorted or malformed retinas.

To fully reveal the polarization properties of the retinal tissues, researchers have been working on incorporating Mueller matrix polarimetry (MMP) into fundus detection. For example, Van Blokland reported a device that takes *in vivo* full Mueller Matrix (MM) measurement of a single retinal location[6]. Bueno has used camera-based MM imaging polarimeters to measure the polarization properties of the cornea, lens and eye[7]. Twietmeyer and Chipman have converted a Carl Zeiss GDx scanning laser partial polarimeter into a MM laser scanning polarimeter[8]. A major disadvantage of these complete polarimeters is their requirement for temporal scanning, in addition to their requirement to collect 16 or more images to reconstruct the MM map of retina, thus limiting the temporal resolution. This leaves the devices vulnerable to eye saccades and increases the amount of work and uncertainty in the image registration post-processing.

In this paper, we present a fundus camera system based on channeled imaging polarimetry (CIP), which could potentially solve the aforementioned problems in current retinal diagnostic devices. The camera system has a snapshot

Polarization Science and Remote Sensing VII, edited by Joseph A. Shaw, Daniel A. LeMaster, Proc. of SPIE Vol. 9613, 96130A · © 2015 SPIE
CCC code: 0277-786X/15/$18 · doi: 10.1117/12.2188480

feature which can greatly decrease the image acquisition time, and make the retinal polarimetry more feasible and affordable. Section 2 briefly explains the optical and opto-mechanical design of the snapshot MM retinal polarimeter. Meanwhile, section 3 describes the system assembly and MM reconstruction strategy. Section 4 shows some preliminary experimental results and other works in progress. Finally, section 5 summarizes the paper.

2. OPTICAL AND OPTO-MECHANICAL DESIGN

Mueller matrix imaging polarimetry has great potential in many application fields including optical testing, remote sensing, quality control and biomedical imaging. Although highly accurate, the traditional rotating element-based Mueller matrix polarimeter has the intrinsic need for taking multiple images during a measurement, which limits the temporal resolution of the devices. Thus, in cases where object motion is frequent, it is often desirable to take the measurement with a single snapshot. Channeled techniques have been widely applied in Stokes polarimetry or imaging polarimetry for these purposes[9-11], but only a small fraction of past work focuses on snapshot full Mueller matrix imaging polarimetry[12-13]. In 2012, Kudenov, Escuti *et al.* theoretically demonstrated the possibility of a Mueller matrix imaging polarimeter based on the channeled imaging polarimetry (CIP) technique, in which spatial frequencies carry the information about Stokes vector parameters of the birefringence target under test[14]. Later, Kudenov and Mallik *et al.* reported the effort towards experimental verification of this theory[15]. Our snapshot retinal imaging Mueller matrix polarimeter (SRIMMP) is based on the same principles. A sketch of system's configuration is as depicted in Figure 1.

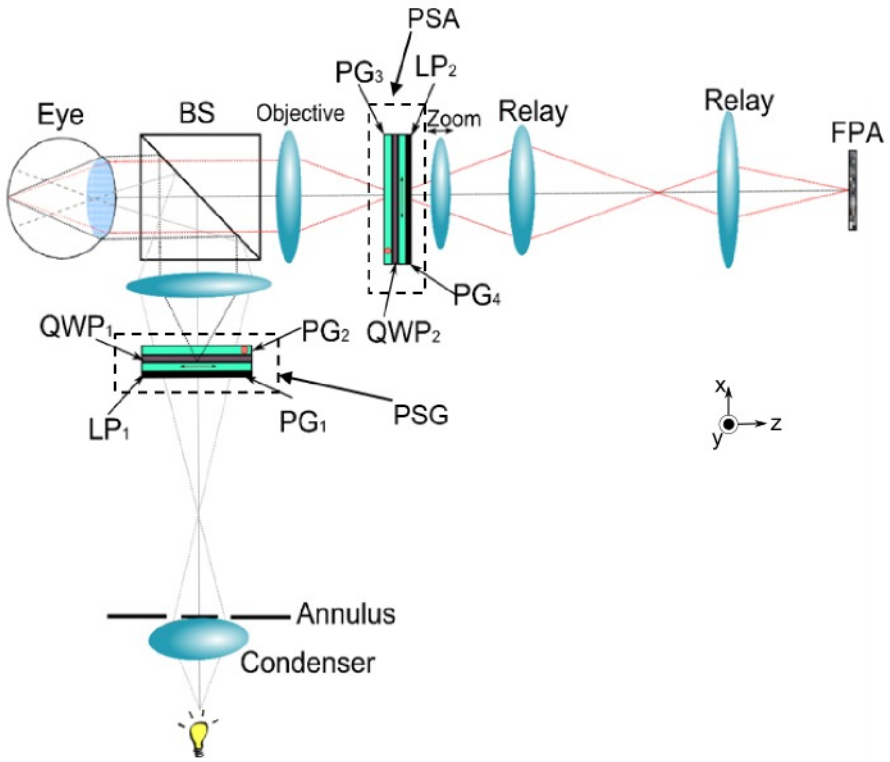

Figure 1. Schematic illustration of the snapshot retinal imaging Mueller matrix polarimeter setup.

In this system, the light from the illumination source is first linearly polarized by polarizer LP_1 before it is transmitted into the polarization state generator (PSG), which consists of 2 polarization gratings (PG_1 and PG_2) and a quarter wave plate (QWP). PG_1 separates the incident beam in two along the *x*-axis (e.g., PG_1's grating vector is parallel to the *z* axis). Due to the PG's birefringence pattern, the two beams generated have orthogonal circular polarization. QWP_1 converts PG_1's orthogonal circular states into orthogonal linear polarization states before being incident on PG_2. PG_2 has its grating vector parallel to the *x* axis, causing a splitting of the two incident linearly polarized beams into a right and left circularly polarized beam (e.g., four beams total). These four beams are then focused onto the retina through a relay lens and beam splitter (BS). The fundus's Mueller matrix information then modulates the frequency components of the incoming illumination. After the light interacts with the retina, the beams are focused onto the polarization state analyzer

(PSA), which is of similar configuration to that of PSG. The beams finally are analyzed by a linear polarizer LP_2 and focused onto a focal plane array (FPA).

Additionally, similar to a conventional fundus camera, an annulus is placed after the condenser lens in the illumination pathway, which conjugates to the cornea of the eye. A circular baffle is placed at the same plane of PSA, to control the field-of-view (FOV) received by FPA as well as to eliminate stray light. As a result, PSG, fundus, PSA and FPA are conjugate to each other, while the annulus is conjugate to the cornea. It is to be noted that an external illumination design has been chosen instead of an internal illumination design. This design choice was made because masks used in an internal illumination system to suppress retroreflections from the objective lens would inevitably block the central field of light on the FPA.

The optical designs were conducted in the sequential mode of Zemax software for both the illumination and imaging pathways to demonstrate that all of the conjugation relations are realized and that the optical performance is satisfactory. The 2D sketches and corresponding diffraction MTF curves of the optical designs are as depicted in Figure 2 for both the illumination and imaging pathways.

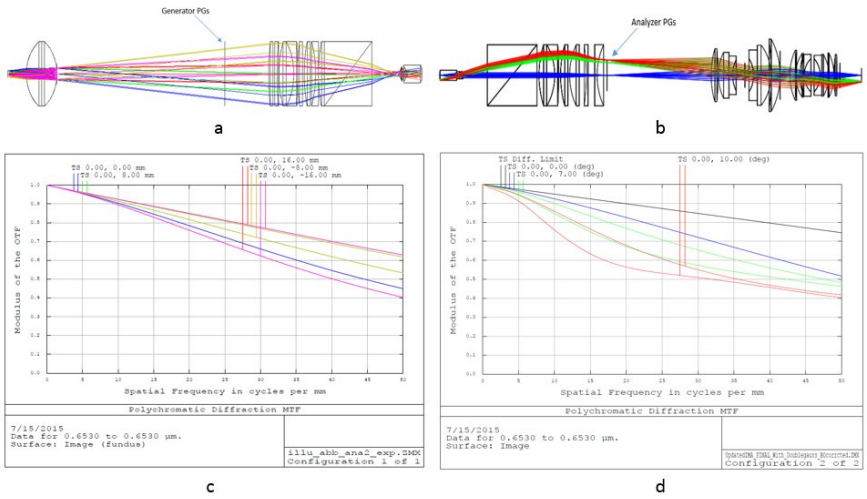

Figure 2. 2D sketches of a) illumination pathway and b) imaging pathway of the SRIMMP system, and the diffraction MTF curves of optics between c) PSG and retina, d) retina and FPA, with 4mm entrance pupil and 653 nm wavelength.

Per the design, the FOV is approximately 30°, while the pupil size is set to 4 mm in diameter. Monochromatic illumination is assumed with a designated wavelength of 653 nm. The design is mainly based on 2 inch optics, with all the lenses available commercially off-the-shelf. Eye relief, or the distance between the eye and the beam splitter, is 25 mm. The tolerancing of both the illumination and imaging pathways was also analyzed in Zemax, and show satisfactory resistance to the potential errors and misalignments during assembly. A non-sequential ray tracing model was also created in the non-sequential mode of Zemax to further verify the power distribution with large scale ray tracing, which also shows good consistency with the design aim. Based upon the optical design, an opto-mechanical design was carried out in Autodesk Inventor 2014. As depicted in Figure 3, the assembly is mounted in a 60 mm cage system, with lens tubes and cage rods to support the whole system. All the mounts can be purchased from Thorlabs except the beamsplitter mount (17). Instead, it was custom fabricated due to tight spacing tolerances with the adjacent lenses.

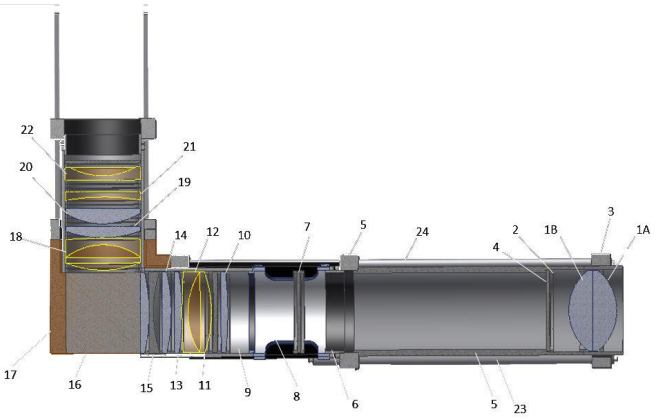

Figure 3. Cross-sectional view of the SRIMMP system assembly in Autodesk Inventor 2014.

3. SYSTEM ASSEMBLY AND MUELLER MATRIX RECONSTRUCTION

System assembly

The system was initially set up on an optical table without the polarization gratings, contained within the PSG and PSA, to perform an initial optical assessment. With this bench-top setup, initial alignment of the optics and illumination safety tests were carried out. As shown in Figure 4, a light emitting diode (LED) was used as the light source. The LED has an optical output power of 1 Watt at a 660 nm peak emission wavelength. Meanwhile, a simple eye model consists of a 25 mm focal length plano-convex lens with a white diffuser placed at the retinal position to simulate a target. Additionally, the annulus pattern, which is projected onto the cornea to avoid corneal reflections, was painted on a 2 inch diameter glass plate, and the plate was inserted into a lens tube. Finally, two commercial camera lenses, with 85 mm and 25 mm focal lengths, were used as relay lenses and transfer the PSA's image from PSA plane to the FPA sensor, which is a USB camera manufactured by Imaging Source.

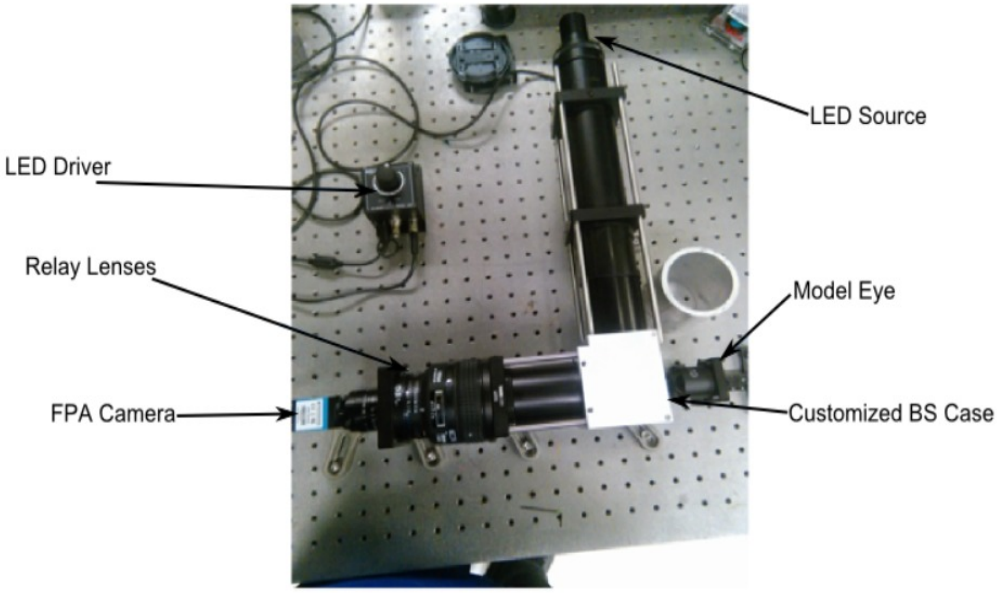

Figure 4. Experimental setup of SRIMMP system on an optical table

To make the system able to take images from a real eye, it must be mounted onto a stage that could move and rotate in 3D space during the tests. For this purpose, a used Kowa FX-50R fundus camera was acquired, which comes with a translation stage that translates along the *x*, *y* and *z* directions, and also rotates in azimuthal and polar directions. Our

device was vertically mounted onto this stage so that the camera's position can be easily adjusted in 3-dimensional space.

With the system on the stage, some initial tests were done to check the fundus imaging capability of our retinal imager. A picture from a dilated eye is shown in Figure 5. As can be seen, the central optic disc and nearby features can be easily distinguished. Small adjustments will be made to improve the imaging performance of this camera, such that more details of the fundus can be revealed. However, it should be noted that the polarimetric imaging technique implemented here trades off spatial resolution for polarimetric resolution; therefore, so long as the general low spatial-frequency features of the optic disc can be resolved, the polarimetric imaging capability can be implemented.

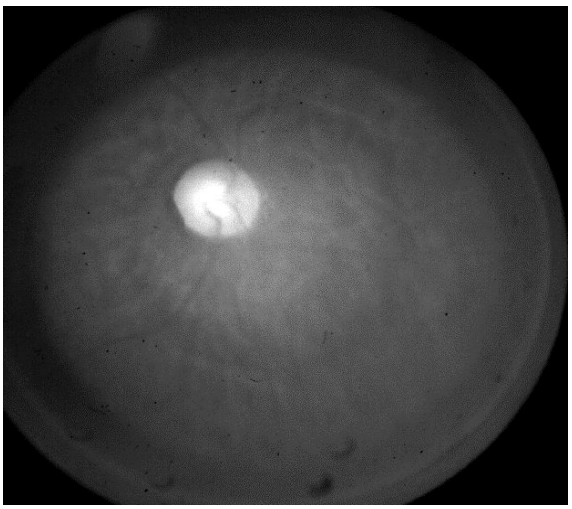

Figure 5. Sample image taken during initial testing of a dilated eye. For this image, no polarimetric fringes are present.

After the initial imaging tests, some upgrades have been done to the system according to some of the issues discovered during the process. The upgraded system is as shown in Figure 6. The most noticeable change is that the illumination pathway is now folded. Instead of a lens tube, the PSG is mounted in a single cage plate at position 1. The space under it, 2, will be taken by the rotating plate for eye lens MTF compensation, which will be discussed in details later this section. A single strap, 3, has replaced the former headrest to provide a more comfortable experience for subjects. The posts of chinrest have also been reinforced by a 5mm aluminum plate, 4. The Imaging Source FPA camera has also been replaced by an AVT Manta camera 5, which has a larger sensing area and better resolution.

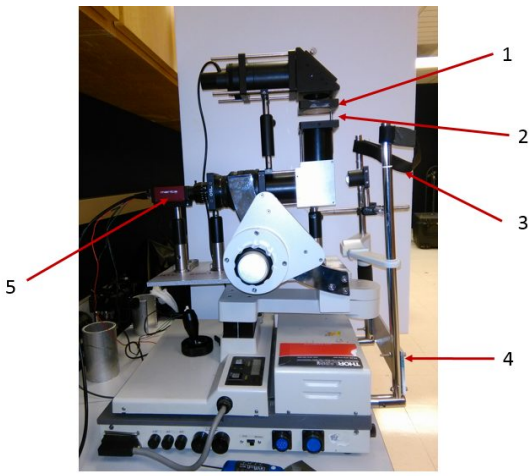

Figure 6. A view of the upgraded fundus imager system

Calibration and Mueller matrix reconstruction

Common methods for calibration include the Fourier transform approach, the inversion matrix approach, and the reference beam approach. In the work of Kudenov and Mallik *et al.*[15], an inversion matrix-based calibration procedure was proposed due to the polarimeter's complexity. However, when the system was calibrated as a singular Mueller matrix polarimeter, small wedge and tilt contained within the calibration elements created significant error in the polarimetric calibration. This complexity stemmed from the fact that the analyzer and generator were coupled. While the spatial resolution and, potentially, the signal-to-noise ratio in this type of situation is more optimal[16], calibration is complex since both the generator and analyzer must be calibrated simultaneously due to the high levels of multiplexing contained within the channels.

In our current work, we have opted instead to incorporate a calibration approach that combines the reference beam and measurement matrix methods. Additionally, a new perspective has been adopted: instead of calibrating the generator and analyzer simultaneously, the PSA and PSG are treated separately. The PSA is first calibrated as a Stokes vector polarimeter alone, while the PSG is later incorporated into the system solely as an incident Stokes vector generator. The calibration procedure is as illustrated in the following section.

First, the PSA's calibration is achieved without the PSG in the system. For the PSA alone, the intensity expression on the FPA is:

$$I(x,y) = S_0(x,y) + S_1(x,y)\cos[2\pi\,\mathrm{U(x+y)}] + S_2(x,y)\sin[2\pi U(x+y)] + S_3(x,y)\cos[2\pi U(\mathrm{y})] \tag{1}$$

where U is the carrier frequency, and S_0, S_1, S_2, S_3 are Stokes coefficients of the sample under test. The magnitude map in the spatial frequency domain is as depicted in Figure 7.

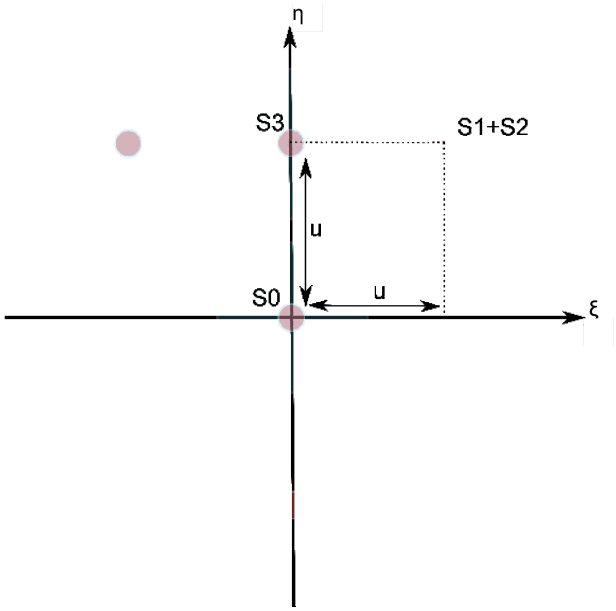

Figure 7. Ideal channel distribution of PSA in Fourier domain, ξ and η are Fourier domain coordinates for x and y.

In frequency domain, three frequency channels C_0, C_1 and C_2 are isolated with 2D filters (the three squares in Figure 7), and the inverse Fourier transform of each is performed separately, resulting in

$$C_0 = S_0(x, y), \tag{2}$$

$$C_1 = \frac{1}{4}[S_1(x, y) + iS_2(x, y)]\mathrm{e}^{i(2\pi Ux + 2\pi Uy)}, \text{ and} \tag{3}$$

$$C_2 = \frac{1}{2}S_3(x, y)\mathrm{e}^{i2\pi Uy}. \tag{4}$$

From equations (2)-(4), it is obvious that the S_0 Stokes parameter can be directly extracted from channel 0, while S_1, S_2 and S_3 are modulated by phase factors within channels 1 and 2, respectively. To retrieve S_1 and S_2, we need to remove (or demodulate) the phase factors. To measure the modulating terms, a linear polarizer, oriented at 0 degrees, is used as the reference sample for channel 1, while a linear polarizer and a quarter wave plate is used as the reference for channel 2. Thus, the corresponding demodulating equations are:

$$S_0(x, y) = \left|C_{0,sample}\right|, \tag{5}$$

$$\frac{S_1(x, y)}{S_0(x, y)} = \mathrm{Re}\left[\frac{C_{1,sample}}{C_{1,reference}} * \frac{C_{0,reference}}{C_{0,sample}}\right], \tag{6}$$

$$\frac{S_2(x, y)}{S_0(x, y)} = \mathrm{Im}\left[\frac{C_{1,sample}}{C_{1,reference}} * \frac{C_{0,reference}}{C_{0,sample}}\right], \text{ and} \tag{7}$$

$$\frac{S_3(x, y)}{S_0(x, y)} = \mathrm{Re}\left[\frac{C_{2,sample}}{C_{2,reference}} * \frac{C_{0,reference}}{C_{0,sample}}\right]. \tag{8}$$

When assembling the PSA, small errors, such as inaccuracy in the retardance and orientation of some optical components, could result in additional channels and channel cross-talk, which need to be compensated for. A general linear polarizer Mueller matrix is defined as

$$\mathbf{M_{LP}}(\theta) = \frac{1}{2}\begin{pmatrix} 1 & \cos 2\theta & \sin 2\theta & 0 \\ \cos 2\theta & \cos^2 2\theta & \sin 2\theta \cos 2\theta & 0 \\ \sin 2\theta & \sin 2\theta \cos 2\theta & \sin^2 2\theta & 0 \\ 0 & 0 & 0 & 0 \end{pmatrix}, \tag{9}$$

where θ represents the orientation of linear polarizer's transmission axis. Meanwhile, a general linear retarder Mueller matrix can be expressed as

$$\mathbf{M_R}(\theta, \delta) = \begin{pmatrix} 1 & 0 & 0 & 0 \\ 0 & \cos^2 2\theta + \cos\delta \sin^2 2\theta & \cos 2\theta \sin 2\theta - \cos 2\theta \cos\delta \sin 2\theta & \sin 2\theta \sin\delta \\ 0 & \cos 2\theta \sin 2\theta - \cos 2\theta \cos\delta \sin 2\theta & \cos\delta \cos^2 2\theta + \sin^2 2\theta & -\cos 2\theta \sin\delta \\ 0 & -\sin 2\theta \sin\delta & \cos 2\theta \sin\delta & \cos\delta \end{pmatrix}, \tag{10}$$

where θ is the angle of the fast axis and δ is the retardance of the retarder. Then the systematic Mueller matrix of the PSA is

$$\mathbf{A}(x,y) \;=\; \mathbf{M}_{\mathbf{LP}}(0)*\mathbf{M}_{\mathbf{R}}(\theta_2(\mathrm{x,y}),180+\varepsilon_3)*\mathbf{M}_{\mathbf{R}}(0,90+\varepsilon_2)*\mathbf{M}_{\mathbf{R}}(\theta_1(\mathrm{x,y}),180+\varepsilon_1), \tag{11}$$

where **A** is the PSA's Mueller matrix, θ_1 is the fast axis orientation of PG_4, θ_2 is the fast axis orientation of PG_3, and ε_1, ε_2, ε_3 are alignment errors. Figure 8 shows the simulated magnitude map in the frequency domain when the first PG, the second PG, and the quarter wave plate in PSA all have 10 degree retardance error.

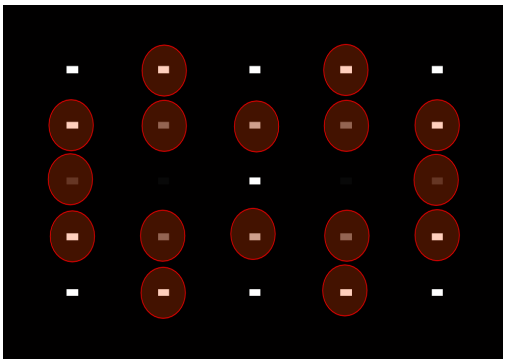

Figure 8. PSA frequency domain magnitude distribution, channels circled are created by defects.

These errors are to be compensated by applying a measurement matrix reference beam calibration technique. It should be noted that 10 degrees of error is much larger than the errors expected for the experimental system, which are more likely to be under 1 degree for each component in the PSA. A possible calibration procedure is sketched in Figure 9. In this procedure, 38 samples with known polarization characteristics are placed at the position of the fundus, one by one, and the corresponding 38 intensity distributions on the FPA plane are measured.

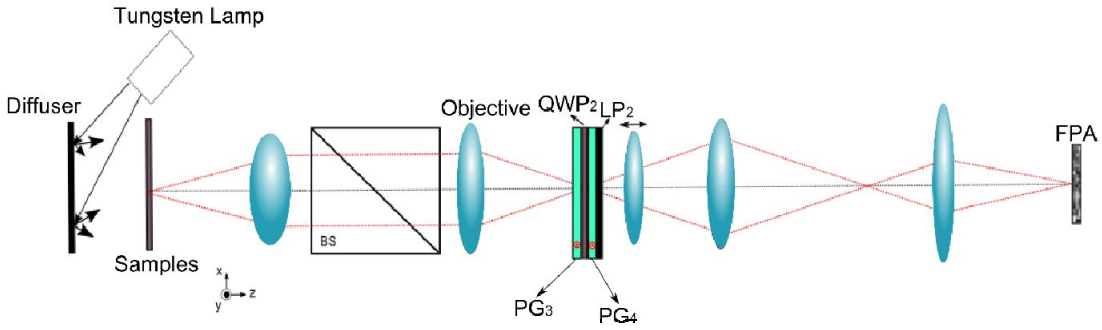

Figure 9. PSA calibration with calibration samples of known polarization states.

Based on the known polarization characteristics of these samples, a 4×38 matrix of nominal Stokes parameters can be formed as

$$S_{nom} = \begin{pmatrix} S_{n0,t1} & S_{n0,t2} & S_{n0,t3} & \dots S_{n0,t38} \\ S_{n1,t1} & S_{n1,t2} & S_{n1,t3} & \dots S_{n1,t38} \\ S_{n2,t1} & S_{n2,t2} & S_{n2,t3} & \dots S_{n2,t38} \\ S_{n3,t1} & S_{n3,t2} & S_{n3,t3} & \dots S_{n3,t38} \end{pmatrix}, \tag{12}$$

where the subscript *ni* refers to the "nominal" or "real" value for the *i = 0, 1, 2, 3* Stokes vectors, and *tj* refers to the *j*th sample. A similar 4×38 matrix of measured Stokes parameters can be formed using the measured Stokes vectors as

$$S_{meas} = \begin{pmatrix} S_{m0,t1} & S_{m0,t2} & S_{m0,t3} & \dots S_{m0,t38} \\ S_{m1,t1} & S_{m1,t2} & S_{m1,t3} & \dots S_{m1,t38} \\ S_{m2,t1} & S_{m2,t2} & S_{m2,t3} & \dots S_{m2,t38} \\ S_{m3,t1} & S_{m3,t2} & S_{m3,t3} & \dots S_{m3,t38} \end{pmatrix}, \tag{13}$$

where the subscript *mj* refers to the *j*th "measured" Stokes parameter. The crosstalk matrix can be modeled via a measurement matrix **W**, which is a 4×4 matrix that maps the measured values to the real values such that

$$\mathbf{W} = \begin{cases} W_{row1} = (pinv(S_{nom}) * S_{meas,column1})^T \\ W_{row2} = (pinv(S_{nom}) * S_{meas,column2})^T \\ W_{row3} = (pinv(S_{nom}) * S_{meas,column2})^T \\ W_{row4} = (pinv(S_{nom}) * S_{meas,column2})^T \end{cases}. \tag{14}$$

where *pinv* means pseudoinverse. The correction matrix W can then be used for calibrating future measurements, as it is the map between measured Stokes vectors and real Stokes vectors. At this point, the calibration of the PSA as a Stokes polarimeter is complete, and the PSA would be able to accurately measure any incoming polarization state.

After calibration of the PSA, the PSG is incorporated into the system. Theoretically speaking, there will be no need to calibrate the PSG. To measure the Mueller matrix of a sample, first, a frame is taken without the eye to extract the incident Stokes vector of each pixel (an "empty polarimeter" measurement). Another frame is then taken with the eye in position, where again, the Stokes vector of each pixel is recorded. The Mueller matrix of a certain spot on the sample is calculated with Stokes vectors before and after the sample over a 30×30 square window.

To quantify the performance of data re-construction, we introduce a metric called averaged absolute error (AAE) here, defined as

$$AAE = \frac{1}{16 L_x L_y} \sum_{i=1}^{4} \sum_{j=1}^{4} abs(\mathrm{M}_{ij} - m_{ij}), \tag{15}$$

where M_{ij} is the coefficient at position *(i,j)* of the nominal Mueller matrix, m_{ij} is the coefficient at position *(i,j)* of the measured Mueller matrix by the system, and L_x and L_y are the width and length of the area being measured, respectively. In other words, it can be seen as the average absolute error at each location of a Mueller matrix.

In a simulation, the test Mueller matrix used is acquired from Shamaraz Firdous' book[17], which is the measured Mueller matrix taken from a scattering turbid sample. A low-frequency variation has been added to the second, third, and fourth rows of the Mueller coefficients to represent the spatial variations,

$$M_{test} = \begin{pmatrix} 0.910 & 0.657 & -0.314 & 0.097 \\ 0.739*\cos[\mathrm{k}(x+y)] & 0.732*\cos[\mathrm{k}(x+y)] & 0.793*\cos[\mathrm{k}(x+y)] & 0.083*\cos[\mathrm{k}(x+y)] \\ 0.435*\cos[\mathrm{k}(x+y)] & 0.243*\cos[\mathrm{k}(x+y)] & 0.620*\cos[\mathrm{k}(x+y)] & -0.213*\cos[\mathrm{k}(x+y)] \\ 0.133*\cos[\mathrm{k}(x+y)] & 0.421*\cos[\mathrm{k}(x+y)] & 0.136*\cos[\mathrm{k}(x+y)] & 0.751*\cos[\mathrm{k}(x+y)] \end{pmatrix} \tag{16}$$

where k represents a low spatial frequency. Simulations show that when retardance error in each birefringence component is not larger than 1°, the overall AAE after calibration would be smaller than 0.01, which is satisfactory.

4. CURRENT WORK AND PRELIMINARY DATA

Experimental results

Preliminary tests have been done without an MTF compensation procedure. The grating periods in PSG and PSA are 1120 μm and 250.8 μm, respectively. Figure 10 below shows an example polarization pattern acquired from one of these tests in which a specular reflector was used as the model eye's target.

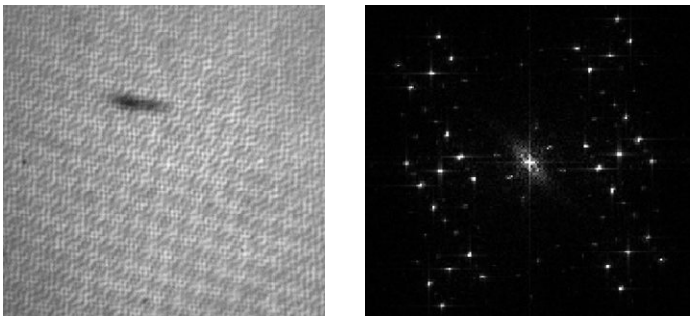

Figure 10. Polarization fringes acquired with a specular reflector as target and corresponding frequency domain pattern.

With a linear polarizer as the target in the model eye, the resulting polarization fringes are as shown in Figure 11. As can be seen, the experimental frame shows good similarity with the simulated fringes. Corresponding frequency domain patterns are as shown in Figure 12. In the frequency domain of the frame taken from the experiment, extra channels can be seen as a result of the misalignments and errors in the experimental system. These raw data need to be calibrated by the aforementioned procedure before conducting Mueller matrix re-construction.

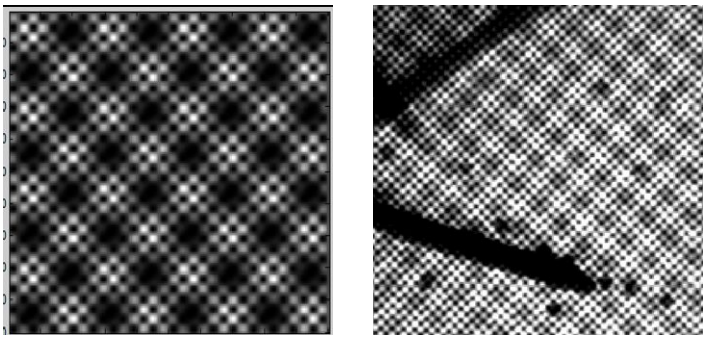

Figure 11. Polarization fringes with linear polarizer as target, left: simulated fringes; right: experimental fringes.

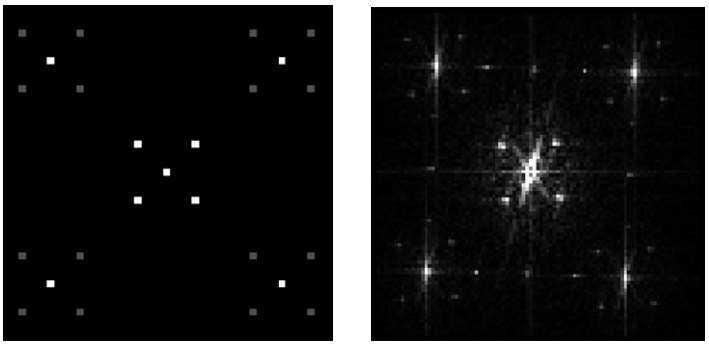

Figure 12. Frequency domain of the fringes in Figure 11, left: simulated; right: experimental.

MTF compensation

The magnitude response of an optical system to spatial frequencies could be described by the modulus transfer function (MTF). While the value of the MTF curve equals to 1 at base frequency, it decreases for higher spatial frequency components. This effect would cause unbalanced sampling among the various channels, we have proposed a method to compensate the MTF as part of the calibration procedure and currently working on it.

Corneal birefringence compensation

Corneal birefringence compensation algorithms have been studied such as bow tie and screen methods[18]. As described in Twietmeyer and Chipman[8], in a Mueller matrix polarimeter, the screen corneal compensation method can be accomplished numerically rather than experimentally. We are working on the Matlab simulation of this calibration

procedure. Implementation of this calibration procedure will occur in parallel with our polarimeter validation and during the post processing of our clinical and animal data.

5. CONCLUSION

In this paper, we have described the design, calibration and preliminary experimental results of our snapshot retinal Mueller matrix polarimeter. Concisely speaking, the concept of a snapshot Mueller matrix retinal imager has been examined and both optical and opto-mechanical designs have been carried out. A prototype has been built in the lab and went through initial tests. Calibration and Mueller matrix reconstruction procedures have been developed and simulation in Matlab shows promising results. Some preliminary pictures have also been taken from the experimental system. In the future, MTF and corneal birefringence compensation schemes will be introduced into the system as part of the calibration procedure. Validation and calibration of the system will be applied experimentally. Finally, some clinical tests will be carried out to further test the device.

ACKNOWLEDGEMENTS

This work was funded by the National Institute of Health under the grant number of 1R21EY022174.

REFERENCES

[1] Quigley, H. A., Broman, A. T., "The number of people with glaucoma worldwide in 2010 and 2020," Br J Ophthalmol. 90:262-267 (2006).
[2] Williams, S., "Diagnosis of Glaucoma," CME Vol.25, No.10, pg 464-468 (2007).
[3] Sommer, A., Miller, N. R., Pollack, I., Maumenee, A. E., and George, T., "The nerve Fiber Layer in the Diagonosis of Glaucoma," Arch Ophthalmol. 95(12):2149-2156 (1977).
[4] "Screening for Glaucoma: Comparative Effectiveness Executive Summary," Agency for Healthcare Research and Quality
[5] Fortune, B., Burgoyne, C. F., Cull, G. and Wang. L., "Onset and Progression of Retinal Nerve Fiber Layer (RNFL) Damage in Experimental Glaucoma Occur Earlier by Scanning Laser Polarimetry (SLP) than by Spectral Domain Optical Coherence Tomography (OCT)," IOVS., Vol.53, 240 (2012).
[6] Klein Brink, H. B., Blokland, G. J., "Birefringence of the human foveal area assessed *in vivo* with Mueller-matrix ellipsometry," J. Opt. Soc. A, Vol.5, No. 1 (1988).
[7] Bueno, J. M., Artal, P., "Double-pass imaging polarimetry in the human eye," Optics Letters, Vol. 24, No. 1 (1999).
[8] Twietmeyer, K. M., Chipman, R. A. *et al*., "Mueller matrix retinal imager with optimized polarization conditions," Optics Express, Vol. 16, No. 26 (2008).
[9] Oka, K. and Kato, T., "Spectroscopic polarimetry with a channeled spectrum," Optics Letters, Vol. 24, No. 21 (1999).
[10] Oka, K. and Kaneko, T., "Compact complete imaging polarimeter using birefringent wedge prisms," Optics Express, Vol. 11, No. 13 (2003).
[11] Oka, K. and Saito, N., "Snapshot complete imaging polarimeter using Savart plates," Proc. SPIE 6295, 629508 (2006).
[12] Hagen, N., Oka, K. and Dereniak, E. L., "Snapshot Mueller matrix spectropolarimeter," Optics Letters, Vol. 32, No. 15 (2007).
[13] Dubreuil, M., Rivet, S., Le Jeune, B. and Cariou, J., "Snapshot Mueller matrix polarimeter by wavelength polarization coding," Optics Express, Vol. 15, No. 21 (2007).
[14] Kudenov, M. K., Escuti, Hagen, N., M. J., Dereniak, E. L. and Oka, K., "Snapshot imaging Mueller matrix polarimeter using polarization gratings," Optics Letters, Vol. 37, No. 8 (2012).
[15] Kudenov, M. W., Mallik, S.*, et al*., "Snapshot Imaging Mueller Matrix Instrument," Proc. SPIE 8897 (2001).
[16] Alenin, A. S., Tyo, J. S., "Generalized channeled polarimetry," JOSA A, Vol. 31, Issue 5 (2014)
[17] Firdous, S., [Laser Tissue Interaction and Wave Propagation in Random Media: Mueller Matrix Polarimetry], Verlag Dr.Muller, Saarbrucken (2010).
[18] Bagga, H., Greenfield, D. S., and Knigbton R. W., "Scanning Laser Polarimetry with Variable Corneal Compensation: Identification and Correction for Corneal Birefringence in Eyes with Macular Disease," IOVS, Vol. 44, No. 5 (2003).